Journal of Hazardous Materials 190 (2011) 133–139

Contents lists available at ScienceDirect

Journal of Hazardous Materials

journal homepage: www.elsevier.com/locate/jhazmat

Characterization and activity of mesoporous titanium dioxide beads with high surface areas and controllable pore sizes☆

Zuoli He*, Zhenfeng Zhu, Junqi Li, Jiaqi Zhou, Na Wei

School of Materials Science and Engineering, Shaanxi University of Science and Technology, Xi'an 710021, PR China

ARTICLE INFO

Article history:
Received 13 January 2011
Received in revised form 3 March 2011
Accepted 4 March 2011
Available online 10 March 2011

Keywords:
Mesoporous
TiO_2 beads
Controllable pore sizes
Photocatalytic
Solvothermal process

ABSTRACT

Mesoporous titanium dioxide beads with high surface areas (over 90 m^2/g) and tunable pore sizes (from 12.8 to 16.5 nm) were synthesized via a solvothermal process heating by microwave irradiation, with ammonia being used as both a source of nitrogen and a control agent for the mesoporous structure. Structural characterization indicated that the mesoporous TiO_2 beads were composed of nanocrystals and pores and the beads possess a optical band gap energy of 3.11 eV. The doping nitrogen was in the form of NH_x or NO_x species and was adsorbed on surface of the beads, which caused changes to the surface electronic structure. The results show that the samples which possess higher-order structure, large surface area and well-defined crystallinity have the best performance in photocatalytic activities exhibited as evaluated in the degradation of methylene blue.

1. Introduction

Mesoporous materials with a crystalline framework, high specific surface area, excellent transport behavior and tunable pore size have received significant research attention [1–4]. To achieve a high surface area and meso or microporous structure, the fabrication of desired morphologies and structures is important as well as control in crystallinity, porosity and composition [5,6]. Titania (TiO_2) has proven to be the most versatile material among various oxide and nonoxide photocatalysts because of its high catalytic activity and long-term stability [7]. Mesoporous titania films [8,9], beads [10–15], networks [16,17], and tubes [18,19] have been prepared via different synthesis strategies. In order to optimize the performance of TiO_2 for the photon-related application, it is desirable to combine high-surface area and surface modified [20,21]. In these applications such as photocatalysis, catalysis, dye-sensitized solar cells (DSSC) and photonic crystals, where the diffusion of photons or molecules through the pore structure is vital for optimum performance, a highly ramified network of macro- and mesopores is desired [22]. Recently, the surface structure of TiO_2 photocatalysts has been intensively explored at the atomic level. And Liu [23] have been made toward creating higher-order and high-surface area micro-sized superstructures from primary anatase TiO_2 nanocrystals via fluoride mediated self-transformation method and proved that surface chemistry of TiO_2 materials open new avenues for the design of advanced photocatalysts with desirable catalytic selectivity beyond reactivity and stability.

Herein we report the synthesis of crystalline, mesoporous TiO_2 beads with surface areas up to 122.2 m^2/g and tunable pore sizes (pore diameters varying from 12.8 to 16.5 nm) through a facile combination of sol–gel and solvothermal processes. This synthetic route of TiO_2 mesoporous beads from amorphous TiO_2 beads has the potential to prepare many spherical materials useful as photocatalytic, gas-sensing, optical, or biomedical materials [24,25]. And higher-order and high-surface area micro-sized superstructures of primary anatase TiO_2 nanocrystals were formed on the surface of mesoporous TiO_2 beads. Additionally, the ammonia used in the synthesis served both as a source for the nitrogen doping as well as a control for the formation of the mesoporous structure. The formation of mesopores and the doping of nitrogen in TiO_2 were completed simultaneously during the solvothermal treatment. The effect of the amount of ammonia on the mesostructure was also discussed.

2. Experimental

2.1. Preparation

Mesoporous TiO_2 beads were prepared from a combined sol–gel and solvothermal process. The compounds used in the synthe-

☆ This research was financially supported by the Doctoral Research Start-up Fund of Shaanxi University of Science and Technology (BJ08-01), Special Fund from Shaanxi Provincial Department of Education (09JK352) and the Graduate Innovation Found of Shaanxi University of Science and Technology.

* Corresponding author. Fax: +86 29 86168802.
E-mail address: wandaohzl@163.com (Z. He).

0304-3894/$ – see front matter © 2011 Elsevier B.V. All rights reserved.
doi:10.1016/j.jhazmat.2011.03.011

sis were tetrabutyl titanate ($Ti(OBu)_4$), ethanol, ammonia, sodium chloride and deionized water.

First, 2.2 mL of $Ti(OBu)_4$ was added dropwise into a mixture of ethanol (100 mL) and sodium chloride solution (0.4 mL 0.1 M) to obtain a turbid solution under magnetic stirring. Then, the suspension was aged in a static condition for 24 h; the powder deposited at the bottom of the vessel was collected and dried at 80 °C in air.

In order to obtain the mesoporous TiO_2 beads with high crystalline frameworks, 0.8 g of the amorphous TiO_2 beads (samples S1) was dispersed into a mixture of 20 mL ethanol and 10 mL deionized water. Then different amounts of 25% ammonia solution were added (0.0, 0.5, 1.0, and 1.5 mL ammonia for samples S2, S3, S4 and S5, respectively). The mixture were sealed within a Teflon-lined autoclave (100 mL) and heated by microwave irradiation at 180 °C for 1 h. The solid products were collected by centrifugation, washed with deionized water and ethanol several times, and then dried in air at 80 °C to produce the final mesoporous TiO_2 beads for characterization.

2.2. Characterization

Morphologies of the samples were observed by using a high-resolution field emission environmental scanning electron microscope (JSM-6700). All the images were obtained under high vacuum mode without sputter coating. X-ray diffraction (D/max-2200, Diffractometer with Cu Ka radiation) was used to verify crystal phase and estimate the crystal sizes of the resulting mesoporous TiO_2 beads. The samples were also analyzed by X-ray photoelectron spectroscopy (XPS). Nitrogen adsorption–desorption isotherms were measured at −196 °C by using a JW-004A system. Fourier transform infrared (FTIR) spectra were taken on a FTIR spectrometer (EQUINOX-55). Absorption spectrum was measured on a UV–vis spectrophotometer (UV-2550) in the wavelength range of 200–800 nm, and the photoluminescence (PL) spectra were measured with a fluorospectrophotometer (HITACHI F-4500) using the 325 nm line of a Xe lamp as the excitation source at room temperature.

The elemental composition of the TiO_2 beads was determined by X-ray photoelectron spectroscopy (XPS) obtained on an Axis Ultra, Kratos (UK) using monochromatic Al Kα radiation (150 W, 15 kV, 1486.6 eV). The vacuum in the spectrometer was 10^{-9} Torr. Binding energies were calibrated relative to the C1s peak (284.8 eV) from hydrocarbons absorbed on the surface of the samples.

2.3. Photocatalytic activity

The photocatalytic activity of the prepared mesoporous TiO_2 beads was evaluated through the degradation of 50 mg/L methyl blue (MB) (marked as −20 min) in a BL-GHX-V multifunctional photochemical reactor (Shanghai Bilon Experiment Equipment Co. Ltd., Shanghai, China). The volume of the reaction solution was 240 mL (8 test tubes of 30 mL) into which 100 mg of photocatalyst was added and stirred for 20 min. Irradiation was provided by a medium-pressure Hg lamp (300 W). The solution was dispersed by sonication, and then transferred to test tubes. Stirring was performed at all the times during the reaction. Sampling was also performed at regular intervals. The residual concentration of MB was determined by measuring its absorbance at 665 nm using an UV–vis spectrophotometer (UV-2550).

3. Results and discussion

3.1. Crystalline structure

Fig. 1 shows the scanning electron microscopy (SEM) images of the TiO_2 beads (sample S1) and the mesoporous TiO_2 beads prepared with different ammonia concentrations, and Fig. 2 shows the X-ray diffraction (XRD) patterns of the compounds. The S1 sample was made up of monodispersed beads with a diameter of about 1000 nm. These beads possessed relatively smooth surfaces without obvious nanocrystalline features (Fig. 1a). The corresponding XRD pattern (Fig. 2, S1) indicates these precursor materials were amorphous.

After solvothermal treatment in a mixture of 20 mL ethanol and 10 mL deionized water, the monodispersed TiO_2 beads possessed an average diameter of 800 nm and with increased roughness (sample S3, Fig. 1b), indicating a 20% shrinkage of bead diameter. As illustrated by the high magnification SEM image (Fig. 1d), these TiO_2 beads contained nanocrystals (16.7 ± 0.8 nm), and pores (≈15 nm) could be observed on the surface of the beads. Additionally, the XRD pattern of these TiO_2 beads (Fig. 2c) shows well-resolved peaks corresponding to anatase as a unique phase (JCPDS card No. 21-1272). Using the Scherrer equation, the crystal size was estimated from the (1 0 1) peak to be 16.88 nm in diameter, which agreed well with the SEM result (Fig. 1e). For samples S3 and S5, the TiO_2 beads that were composed of elongated TiO_2 nanocrystals

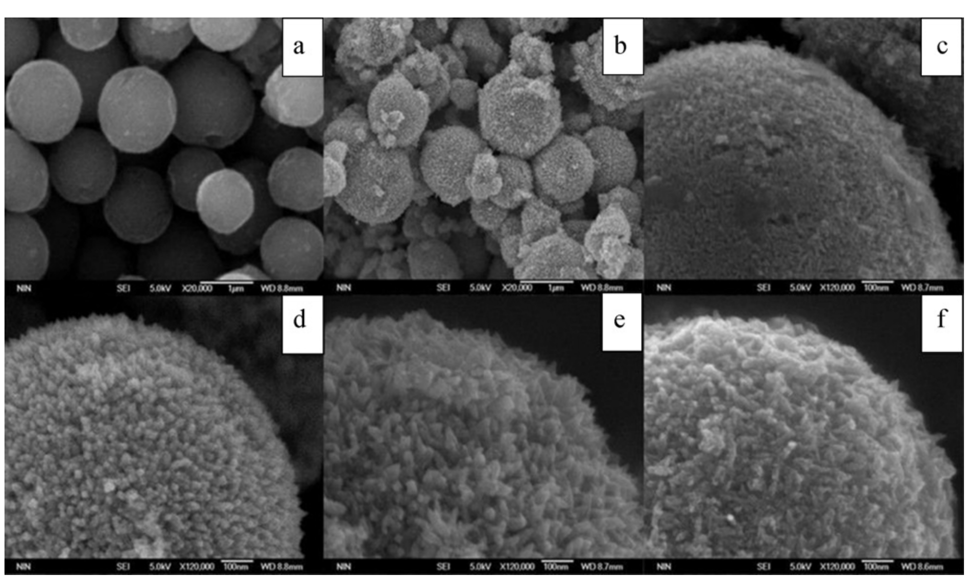

Fig. 1. SEM images of the precursor material S1 (a), and the mesoporous TiO_2 beads S2 (c), S3 (b), (d), S4 (e) and S5 (f).

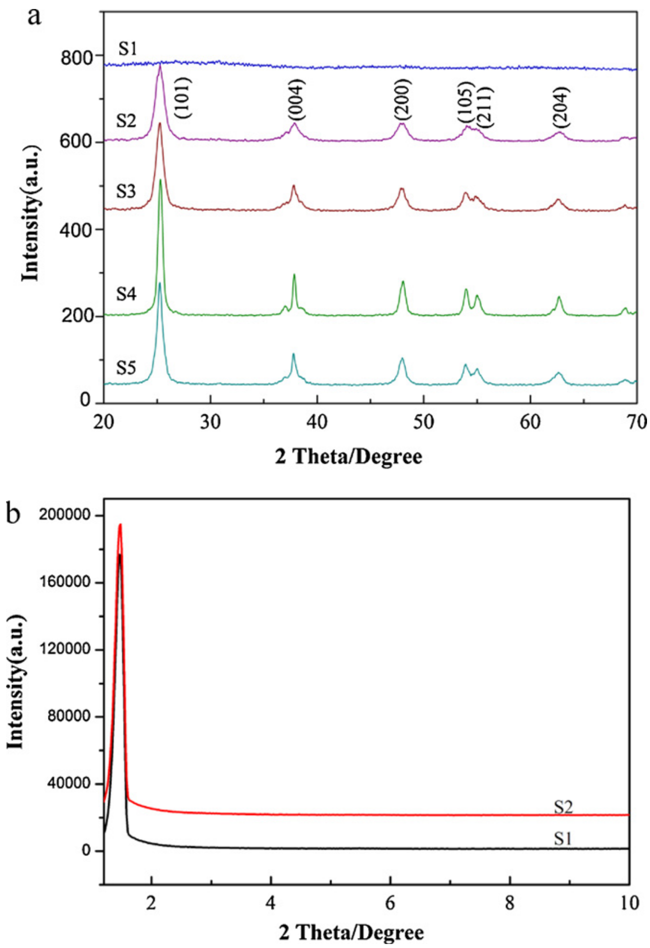

Fig. 2. (a) Wide-angle XRD patterns of the as-synthesized TiO_2 beads (samples S1, S2, S3, S4 and S5) and (b) low-angle XRD patterns of sample S1 and S2.

(Fig. 1e and f) with an average particle size of (20.0 ± 0.8) and (18.0 ± 1.0) nm (short dimension), respectively. Compared to sample S2 (Fig. 1c), the crystal size was increased due to the presence of ammonia during the solvothermal process, which instigated oriented crystal growth to give rise to the elongated nanocrystals. However, when excessive ammonia was added, such as for S5 (Fig. 1f), the mixture resulted in monodisperse TiO_2 beads that were slightly smaller in their oriented crystal growth compared to S4.

It has been confirmed that conventional methods such as sol–gel could not be used to prepare monodispersed spherical titania because the hydrolysis rate of Ti-containing precursors was too fast and the nucleation and the growth were difficult to separate. In the present research, the $Ti(OBu)_4$/NaCl/ethanol mixture, a quasi-nonaqueous system, slowed the initiation of the alcoholysis of $Ti(OBu)_4$ at the ambient temperature. The concentration of mineralizing agent (NaCl in here) controlled the slow nucleation and growth processes of TiO_2 to form small TiO_2 crystallites. Then, these nanometer-sized particles aggregated isotropically to form the micrometer-sized spherical product due to a well-known aggregation mechanism [26,27]. The mesopores were formed from the intercrystallite void that originated from the loose aggregation of the nanoparticles, thus explaining why sample S1 had a mesoporous structure (as shown in Fig. 2b).

However, during the solvothermal process of the mixture, the amorphous TiO_2 beads were partly redecomposed into nanoparticles and then aggregated to produce the formation of TiO_2 nuclei. The TiO_2 nuclei were formed and grew on the malformed surface of beads. By aging for 1 h, the mesoporous TiO_2 beads were

Table 1
Physical properties of the as-synthesized TiO_2 beads.

Sample	Nitrogen content (at%)[a]	Surface areas (m^2/g)	Pore size (nm)	d_{XRD}[b] (nm)	D_{SEM}[c] (nm)
S2	0.05	122.2 ± 0.5	12.8 ± 0.2	10.40	10.5 ± 0.3
S3	0.54	107.0 ± 0.7	14.2 ± 0.2	11.75	16.7 ± 0.5
S4	0.91	90.1 ± 0.6	16.5 ± 0.3	16.88	20.0 ± 0.8
S5	1.34	94.2 ± 0.8	15.1 ± 0.2	13.64	18.0 ± 1.0

[a] Nitrogen content (at%) calculated from XPS.
[b] Crystal size calculated by apply the Scherrer equation to the (1 0 1) anatase peak.
[c] Crystal size measured from the corresponding SEM images (Fig. 1c–f).

formed finally. In this paper, the addition of ammonia can cause a large quantity of gas such as NH_3 to be produced in the autoclave and increase the pH in the solution. More ammonia in the starting solution led to an increase in the number of nuclei formed at the beginning period of solvothermal treatment. Thus, TiO_2 crystallite size would be limited since the total amount of TiO_2 in solution is the same, which could be used to explain the difference in crystallite size of the products. These larger amounts of nuclei and then the small crystallites in the larger amount of the ammonia-added products (such as S4, S5) made the aggregation process faster and more random [28]. Therefore, the samples S4 and S5 have a larger nanocrystals size and mesopore size.

3.2. XPS analysis

The XPS analysis in Fig. 3a shows that S4 consisted of Ti, O, C and N; the C was mainly ascribed to adventitious hydrocarbon from XPS itself. Fig. 3b shows the XPS spectra of the N 1s region while Fig. 3c and d represents the O 1s and the Ti 2p region respectively. The N 1s spectrum indicates one peak of binding energy around 400 eV, which most of the researchers interpret the peaks above 400 eV as the chemisorbed γ-N_2 or from surface adsorbed NH_x species or from NO_x [29,30], though there is still some controversy over the exact position of N in N-doped TiO_2. The O 1s XPS spectrum exhibited an additional peak at a slightly higher BE than TiO_2 which was indicative of the incorporation of N in TiO_2. The O 1s region could be fitted by the peak at 531.3 eV corresponding to the Ti–O bond (Fig. 3c) [31]. Finally, in Fig. 3d the peak position of Ti 2p3/2 corresponds to that of the Ti^{4+} oxidation state. The shape of the Ti 2p excludes the presence of traceable amount of Ti^{4+}, which are separated by about 5.7 eV formed the Ti^{4+} peak [32].

The atomic content of nitrogen in the samples was calculated from the XPS and is represented in Table 1. S3, S4 and S5 had N contents of 0.54, 0.91, and 1.34 atomic%, respectively.

3.3. BET analysis

Fig. 4 shows the nitrogen adsorption–desorption isotherm (inset) and pore size distribution plots for the mesoporous TiO_2 beads (sample S4). The hysteresis loop is of type H2, which is consistent with pores with narrow necks and wider bodies (ink-bottle pores) [21], and indicates the presence of mesoporous materials according to IUPAC classification [26]. The plot of the pore size distribution was determined by using the Barrett–Joyner–Halenda (BJH) method from the desorption branch of the isotherm. The average pore diameter and BET surface area of the TiO_2 beads are 16.5 nm and 90.1 m^2/g, respectively. The results of other samples are shown in Table 1. As shown in Table 1, the surface areas for samples S2, S3, S4, and S5 were all larger than 90 m^2/g and there were obvious porous characteristics and mesoporous structure.

The sample S2 had a specific surface area about 122 m^2/g and a narrow pore size distribution centered at 12.8 nm. Adding 0.5 and 1.5 mL ammonia solution resulted in the pore size increasing to 14.2 and 15.1 nm for samples S3 and S5, respectively. This enlargement

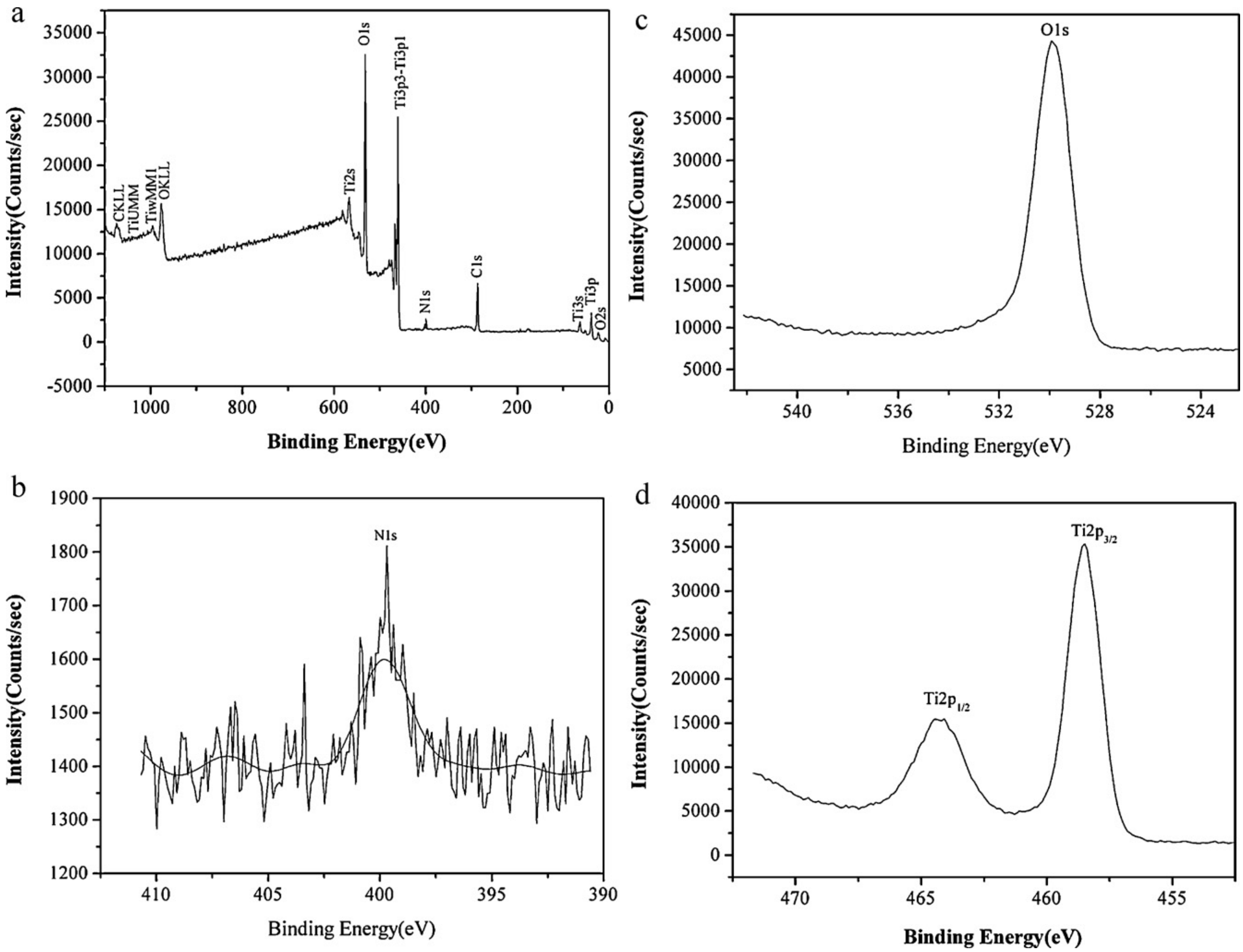

Fig. 3. (a) The survey spectrum; (b) N1s XPS spectra; (c) O1s XPS spectra and (d) Ti2p XPS spectra of sample S4.

in pore size along with an increase in crystal size resulted in a corresponding decrease in the specific surface area from 107.0 to 90.1 and 94.2 m^2/g in this process. And the sample S5 have letter larger than sample S4 because of the smaller size of the nanocrystals (see Fig. 2a and Table 1).

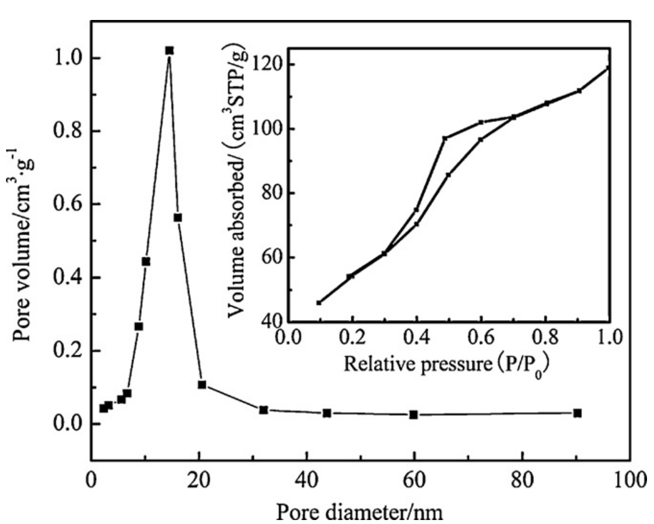

Fig. 4. N_2-sorption isotherms (inset) and corresponding pore-size distribution curves for the TiO_2 beads (sample S4).

3.4. FTIR analysis

The FT-IR spectra of the mesoporous TiO_2 beads (sample S2, S3, S4, S5) are shown in Fig. 5a and b. The broad peaks at 3400 and 1650 cm^{-1} observed for two TiO_2 samples correspond to the bending and stretching models of surface-adsorbed water and hydroxyl groups, respectively [33]. This indicates that water molecules are easily adsorbed on the surface of TiO_2 [34]. The 700–460 cm^{-1} range has a broad and flat absorption band due to the quantum effect of nano-particle size which causes the fine structure of the infrared absorption band to disappear [35,36]. Additionally, peaks characteristic of Ti–O stretching vibrations occurred around 480 cm^{-1}. The FTIR spectra of plasma showed a new peak at 1404 cm^{-1} which was absent in the samples S3, S4, S5 and can be attributed to the C–H deformation vibration of CH_3–N from the ammonia solution.

3.5. UV–vis analysis

The optical band gap of the mesoporous TiO_2 beads was tested by means of UV–vis optical absorbance spectroscopy. The relationship between the absorption coefficient (α) and the photon energy ($h\nu$) can be written as shown in Eq. (1) [27]:

$$(\alpha h\nu)^2 = B(E - E_g) \quad (1)$$

where B is the constant related to the effective masses associated with the valence and conduction bands, E_g is the band gap energy,

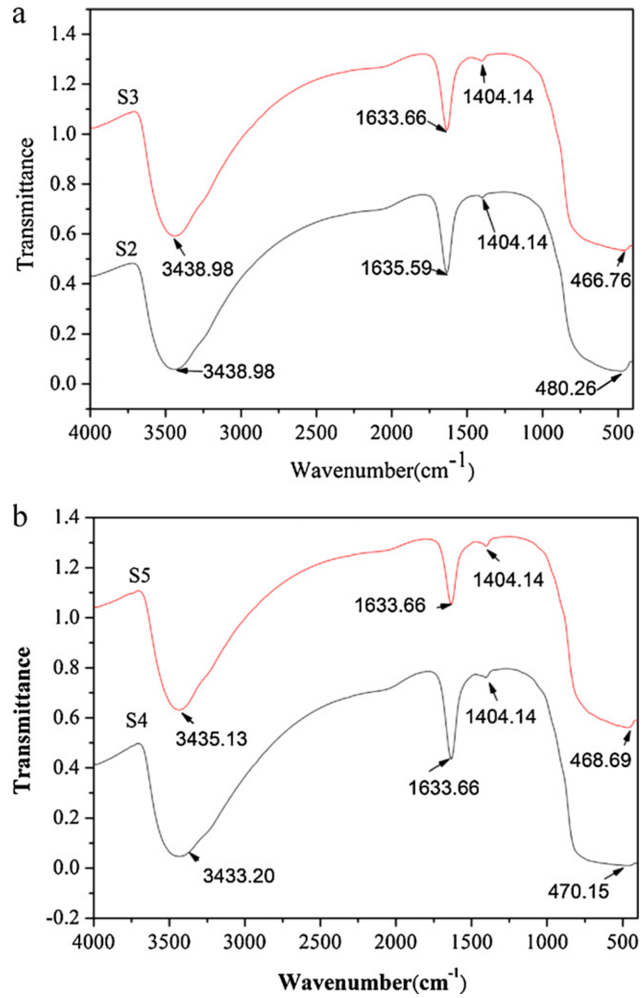

Fig. 5. FTIR spectrums of the samples.

and E is the photon energy as defined by $E = h\nu$. Fig. 6 shows the absorption spectra of the samples, which are all nearly identical, indicating that their optical band gaps were also almost the same. The inset curve shows the plots of $(\alpha h\nu)^2$ versus the $(h\nu)$. E_g for the mesoporous TiO_2 beads can be calculated by extrapolating the linear portion of $(\alpha h\nu)^2$ versus the $(h\nu)$ plot to $\alpha = 0$. Thus, the optical band gap for these mesoporous TiO_2 beads is about 3.11 eV.

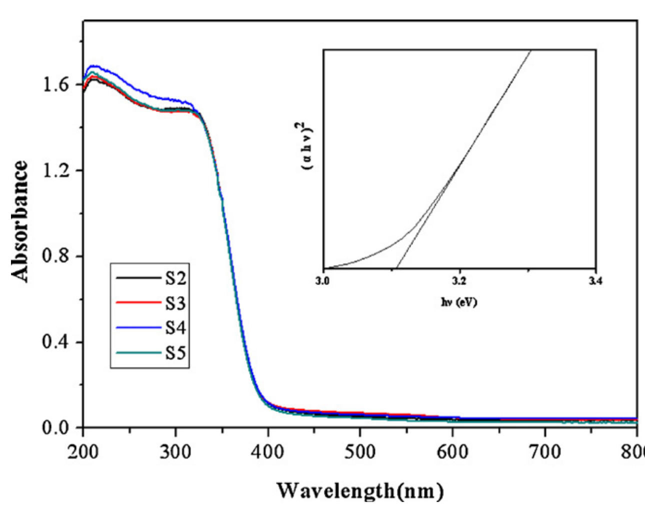

Fig. 6. UV–vis absorbance spectrum of the TiO_2 beads, The inset shows the plot of $(\alpha h\nu)^2$ versus photon energy $(h\nu)$.

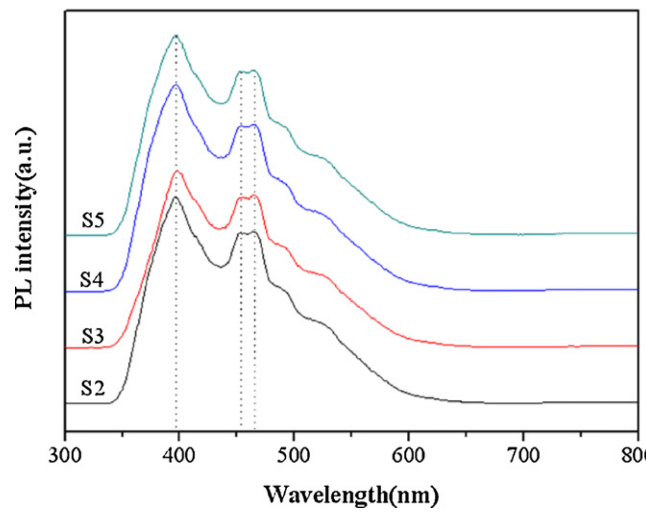

Fig. 7. The photoluminescence (PL) spectra of the samples.

3.6. PL analysis

PL emission spectra have been widely used to investigate the efficiency of charge carrier trapping, immigration, and transfer, and to understand the fate of electron–hole pairs in semiconductor particles. In this study, PL spectra of the samples are shown in Fig. 7 revealing that the PL peaks are nearly identifical in shape and position for all of the samples. There was a broad emission band centered at 396 nm which was ascribed to bound-exciton emission due to the trapping of free excitons by titanate groups near defects. There were also PL bands at the long wavelength range from 440 to 520 nm, which were attributed to the oxygen vacancies, impurities and defects. However, when the amount of 25% ammonia solution was higher than 0.5 mL, the pore sizes increased accordingly which encourages surface recombination. Thus the peak at 396 nm became stronger, and the peak at 468 nm only changed slightly. Lastly, the PL spectra clearly showed that the additions of ammonia can affect the surface electronic structure, and the doping nitrogen was in the form of NH_x or NO_x species adsorbed on surface of the beads [37].

3.7. Photocatalytic activity

The photocatalytic activity of the prepared samples was evaluated by monitoring the degradation of MB in aqueous solution. Fig. 8 shows successive UV–vis spectra of the MB photocatalytic degradation in the presence of the sample S2 under UV irradiation, and Fig. 9 shows the photocatalytic degradation of by all of the samples. A progressive decrease in the MB absorption band at 665 nm is clearly shown in Fig. 8 when the solution exposed to UV illumination. No changes in absorbance at 665 nm are observed in the dark or in the absence of the TiO_2 samples, indicating that the highly crystallized mesoporous TiO_2 beads exhibit good photocatalytic activity. The mesoporous sample exhibits photocatalytic activity that was marginally better than S1, because of the anatase phase structure and high BET surface area. Moreover, hydrothermal synthesis is proven to be an effective method to enhance the photocatalytic activity of nano-sized TiO_2 materials. Interestingly, changes in the addition of ammonia exhibit a significant influence on the photocatalytic activity of the TiO_2 samples (Fig. 9), due to increased crystallization, formation of the mesoporous structure and surface modified. This result also demonstrated that the samples possessed high surface area and better quantum-size effects, which could change the surface electronic structure to shorten the

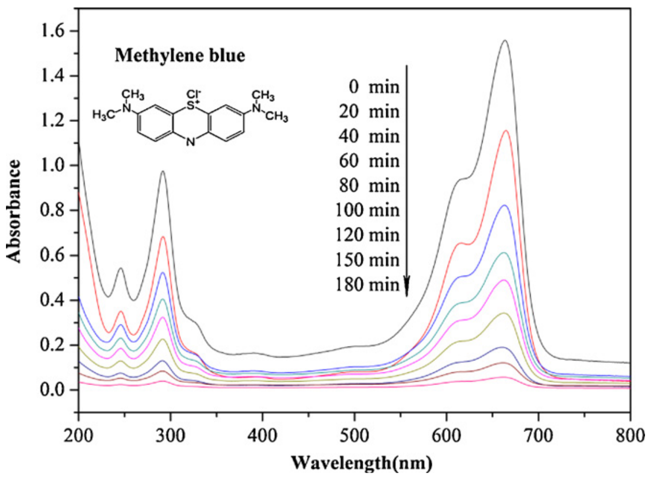

Fig. 8. Successive UV–vis spectra of MB photocatalytic degradation in the presence of S2 sample under UV irradiation. The concentration of the reactants was as follow: [MB] = 50 mg/L, [S2] = 0.1 g/L.

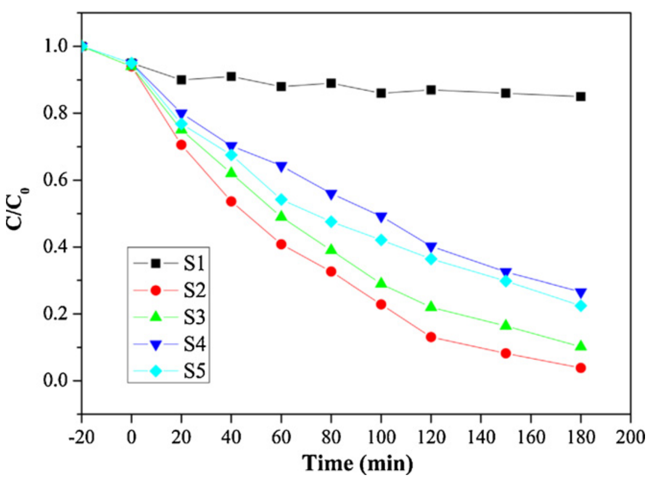

Fig. 9. Photocatalytic degradation activity of different samples.

route for an electron to migrate from the conduction band to its surface and enhance the activities of the electrons and holes [24,25].

In general, specific surface areas and crystallinity can be conflicting factors influencing the photo-catalytic reactivity of TiO_2 [38,39], particularly for amorphous and poorly crystalline materials in which the enhanced activity associated with large surface areas is offset by increased numbers of defects that promote photogenerated electron–hole recombination and reduce photoactivity. The photocatalytic activity is therefore mainly related to a balance between the specific surface area and crystallinity, the sample S2 is optimized because of the higher-order structure, relatively large surface area and well-defined anatase crystallinity that reduce electron–hole recombination. So the sample S4 have the highly crystallinity and relative smaller surface areas, show lower photocatalytic activity than the sample S2 and these samples exhibit the high specific photocatalytic activity also (see Fig. 9).

4. Conclusions

In summary, we have successfully demonstrated highly crystallized mesoporous TiO_2 beads with high surface areas of up to 122.2 m^2/g and tunable pore sizes (from 12.8 to 16.5 nm) prepared through a combined sol–gel and solvothermal process heated by microwave irradiation. In this process, ammonia had a crucial effect on the mesoporous structure and the nitrogen doping amount in TiO_2; the surface electronic structure changed due to the nitrogen doping shown in the PL spectra. The photocatalytic results also proved that the sample S2 has the best performance in photocatalytic degradation because of the higher-order structure, relatively large surface area and well-defined anatase crystallinity that reduce electron–hole recombination.

Acknowledgements

This research was financially supported by the Doctoral Research Start-up Fund of Shaanxi University of Science and Technology (BJ08-01), Special Fund from Shaanxi Provincial Department of Education (09JK352) and the Graduate Innovation Fund of Shaanxi University of Science and Technology.

References

[1] P.D. Yang, D.Y. Zhao, D.I. Margolese, B.F. Chmelka, G.D. Stucky, Block copolymer templating syntheses of mesoporous metal oxides with large ordering lengths and semicrystalline framework, Chem. Mater. 11 (1999) 2813–2826.
[2] J. Lee, M.C. Orilall, S.C. Warren, M. Kamperman, F.J. Disalvo, U. Wiesner, Direct access to thermally stable and highly crystalline mesoporous transition-metal oxides with uniform pores, Nat. Mater. 7 (2008) 222–228.
[3] W.Y. Dong, Y.J. Sun, C.W. Lee, W.M. Hua, X.C. Lu, Y.F. Shi, S.C. Zhang, J.M. Chen, D.Y. Zhao, Controllable and repeatable synthesis of thermally stable anatase nanocrystal-silica composites with highly ordered hexagonal mesostructures, J. Am. Chem. Soc. 129 (2007) 13894–13904.
[4] H.S. Zhou, D.L. Li, M. Hibino, I. Honma, A self-ordered, crystalline-glass, mesoporous nanocomposite for use as a lithium-based storage device with both high power and high energy densities, Angew. Chem. Int. Ed. 44 (2005) 797–802.
[5] H.G. Yang, C.H. Sun, S.Z. Qiao, J. Zou, G. Liu, S.C. Smith, H.M. Cheng, G.Q. Lu, Anatase TiO_2 single crystals with a large percentage of reactive facets, Nature 453 (2008) 638–641.
[6] Z.S. Wang, H. Kawauchi, T. Kashima, H. Arakawa, Significant influence of TiO_2 photoelectrode morphology on the energy conversion efficiency of N719 dye-sensitized solar cell, Coord. Chem. Rev. 248 (2004) 1381–1389.
[7] Y.B. Liu, X.J. Gan, B.X. Zhou, B.T. Xiong, J.H. Li, C.P. Dong, J. Bai, W.M. Cai, Photoelectrocatalytic degradation of tetracycline by highly effective TiO_2 nanopore arrays electrode, J. Hazard. Mater. 171 (2009) 678–683.
[8] J.H. Schattka, E.H.M. Wong, M. Antonietti, R.A. Caruso, Sol–gel templating of membranes to form thick, porous titania, titania/zirconia and titania/silica films, J. Mater. Chem. 16 (2006) 1414–1420.
[9] S.Y. Choi, M. Mamak, N. Coombs, N. Chopra, G.A. Ozin, Thermally stable two-dimensional hexagonal mesoporous nanocrystalline anatase, meso-nc-TiO_2: bulk and crack-free thin film morphologies, Adv. Funct. Mater. 14 (2004) 335–344.
[10] A.G. Dong, N. Ren, Y. Tang, Y.J. Wang, Y.H. Zhang, W.M. Hua, Z. Gao, General synthesis of mesoporous spheres of metal oxides and phosphates, J. Am. Chem. Soc. 125 (2003) 4976–4977.
[11] D.G. Shchukin, R.A. Caruso, Template synthesis and photocatalytic properties of porous metal oxide spheres formed by nanoparticle infiltration, Chem. Mater. 16 (2004) 2287–2292.
[12] N. Lakshminarasimhan, E. Bae, W. Choi, Enhanced photocatalytic production of H_2 on mesoporous TiO_2 prepared by template-free method: role of interparticle charge transfer, J. Phys. Chem. C 111 (2007) 15244–15250.
[13] J.B. Yin, L.Q. Xiang, X.P. Zhao, Monodisperse spherical mesoporous Eu-doped TiO_2 phosphor particles and the luminescence properties, Appl. Phys. Lett. 90 (2007) 1131121–1131123.
[14] L. Yang, Y. Lin, J.G. Jia, X.R. Xiao, X.P. Li, X.W. Zhou, Light harvesting enhancement for dye-sensitized solar cells by novel anode containing cauliflower-like TiO_2 spheres, J. Power Sources 182 (2008) 370–376.
[15] Y.G. Guo, Y.S. Hu, J. Maier, Synthesis of hierarchically mesoporous anatase spheres and their application in lithium batteries, Chem. Commun. (2006) 2783–2785.
[16] R.A. Caruso, M. Antonietti, M. Giersig, H.P. Hentze, J.G. Jia, Modification of TiO_2 network structures using a polymer gel coating technique, Chem. Mater. 13 (2001) 1114–1123.
[17] J.F. Zhou, M.F. Zhou, R.A. Caruso, Agarose template for the fabrication of macroporous metal oxide structures, Langmuir 22 (2006) 3332–3336.
[18] K.X. Wang, M.D. Wei, M.A. Morris, H.S. Zhou, J.D. Holmes, Mesoporous titania nanotubes: their preparation and application as electrode materials for rechargeable lithium batteries, Adv. Mater. 19 (2007) 3016–3020.
[19] X. Wu, Q.Z. Jiang, Z.F. Ma, W.F. Shangguan, Tile overlapping model for synthesizing TiO_2 nanotubes by microwave irradiation, Solid State Chem. 143 (2007) 343–347.
[20] J.K. Zhou, L. Lv, J.Q. Yu, H.L. Li, P.Z. Guo, H. Sun, X.S. Zhao, Synthesis of self-organized polycrystalline F-doped TiO_2 hollow microspheres and their photocatalytic activity under visible light, J. Phys. Chem. C 112 (2008) 5316–5321.

[21] J.G. Yu, Q.J. Xiang, J.R. Ran, S. Mann, One-step hydrothermal fabrication and photocatalytic activity of surface-fluorinated TiO_2 hollow microspheres and tabular anatase single micro-crystals with high-energy facets, Cryst. Eng. Commun. 12 (2010) 872–879.

[22] W.K. Ho, J.C. Yu, S.C. Lee, Synthesis of hierarchical nanoporous F-doped TiO_2 spheres with visible light photocatalytic activity, Chem. Commun. (2006) 1115–1117.

[23] S.W. Liu, J.G. Yu, M. Jaroniec, Tunable photocatalytic selectivity of hollow TiO_2 microspheres composed of anatase polyhedra with exposed {0 0 1} facets, J. Am. Chem. Soc. 132 (2010) 11914–11916.

[24] R. Asahi, T. Morikawa, T. Ohwaki, K. Aoki, Y. Taga, Visible-light photocatalysis in nitrogen-doped titanium oxides, Science 293 (2001) 269–271.

[25] H. Irie, Y. Watanabe, K. Hashimoto, Nitrogen-concentration dependence on photocatalytic activity of $TiO_{2-x}N_x$ powders, J. Phys. Chem. B 107 (2003) 5483–5486.

[26] C. Boissiere, A. van der Lee, A. El Mansouri, A. Larbot, E. Prouzet, A double step synthesis of mesoporous micrometric spherical MSU-X silica particles, Chem. Commun. (1999) 2047–2048.

[27] M. Ocana, R. Rodriguez-Clemente, C.J. Serna, Uniform colloidal particles in solution: formation mechanisms, Adv. Mater. 7 (2004) 212–216.

[28] B. Chi, L. Zhao, T. Jin, One-step template-free route for synthesis of mesoporous N-doped titania spheres, J. Phys. Chem. C 111 (2007) 6189–6193.

[29] K.S.W. Sing, Reporting physisorption data for gas/solid systems with special reference to the determination of surface area and porosity (Provisional), Pure. Appl. Chem. 54 (1982) 2201–2218.

[30] R.A. Van Leeuwen, C.J. Hung, D.R. Kammler, J.A. Swizer, Optical and electronic transport properties of electrodeposited thallium(III) oxide films, J. Phys. Chem. 99 (1995) 15247–15252.

[31] J. Ananpattarachai, P. Kajitvichyanukul, S. Seraphin, Visible light absorption ability and photocatalytic oxidation activity of various interstitial N-doped TiO_2 prepared from different nitrogen dopants, J. Hazard. Mater. 168 (2009) 253–261.

[32] Y.K. Lai, J.Y. Huang, H.F. Zhang, V.P. Subramaniam, Y.X. Tang, D.G. Gong, L. Sundar, L. Sun, Z. Chen, C.J. Lin, Nitrogen-doped TiO_2 nanotube array films with enhanced photocatalytic activity under various light sources, J. Hazard. Mater. 184 (2010) 855–863.

[33] J.C. Yu, W.K. Ho, J.G. Yu, S.K. Hark, K. Lu, Effects of trifluoroacetic acid modification on the surface microstructures and photocatalytic activity of mesoporous TiO_2 thin films, Langmuir 19 (2003) 3889–3896.

[34] J.G. Yu, L. Shi, One-pot hydrothermal synthesis and enhanced photocatalytic activity of trifluoroacetic acid modified TiO_2 hollow microspheres, J. Mol. Catal. A: Chem. 326 (2010) 8–14.

[35] Y.M. Hu, A.M. Yang, J.Z. Xiang, M.Q. Li, J.H. Fang, X.Q. Zhang, X.H. Wu, Study on infrared absorbency of superfine TiO_2 grain, Infrared Technol. 25 (2003) 60–62 (in Chinese).

[36] Z.F. Zhu, Z.L. He, J.Q. Li, D.G. Liu, N. Wei, Synthesis and characterization of fluorinated TiO_2 microspheres with novel structure by sonochemical-microwave hydrothermal treatment, Mater. Res. Innov. 5 (2010) 426–430.

[37] B.S. Liu, X.J. Zhao, Q.N. Zhao, X. He, J.Y. Feng, Effect of heat treatment on the UV–vis–NIR and PL spectra of TiO_2 films, J. Electron. Spectrosc. Relat. Phenom. 148 (2005) 158–163.

[38] O. Carp, C.L. Huisman, A. Reller, Photoinduced reactivity of titanium dioxide, Prog. Solid State Chem. 32 (2004) 33–177.

[39] J.G. Yu, G.H. Wang, B. Cheng, M.H. Zhou, Effects of hydrothermal temperature and time on the photocatalytic activity and microstructures of bimodal mesoporous TiO_2 powders, Appl. Catal. B 69 (2007) 171–180.